Non-contrast free-breathing liver perfusion imaging using velocity selective ASL combined with prospective motion compensation ☆

Ke Zhang [a,b,c,d], Simon M.F. Triphan [a,b,c], Mark O. Wielpütz [a,b,c], Christian H. Ziener [d], Mark E. Ladd [e,f,g], Heinz-Peter Schlemmer [d], Hans-Ulrich Kauczor [a,b,c], Oliver Sedlaczek [a,c,d], Felix T. Kurz [d,h,*]

[a] Department of Diagnostic & Interventional Radiology, Heidelberg University Hospital, Heidelberg, Germany
[b] Translational Lung Research Center (TLRC), German Center for Lung Research (DZL), Heidelberg, Germany
[c] Department of Diagnostic & Interventional Radiology with Nuclear Medicine, Thoraxklinik at Heidelberg University Hospital, Heidelberg, Germany
[d] Divison of Radiology, German Cancer Research Center, Heidelberg, Germany
[e] Divison of Medical Physics in Radiology, German Cancer Research Center, Heidelberg, Germany
[f] Faculty of Physics and Astronomy, Heidelberg University, Heidelberg, Germany
[g] Faculty of Medicine, Heidelberg University, Heidelberg, Germany
[h] Division of Neuroradiology, Geneva University Hospitals, Geneva, Switzerland

Received 12 February 2024; accepted 11 June 2024

Abstract

Purpose: To apply velocity selective arterial spin labeling (VSASL) combined with a navigator-based (NAV) prospective motion compensation method for a free–breathing liver perfusion measurement without contrast agent.
Methods: Sinc-modulated Velocity Selective Inversion (sinc-VSI) pulses were applied as labeling and control pulses. In order to account for respiratory motion, a navigator was employed in the form of a single gradient-echo projection read-out, located at the diaphragm along the inferior-superior direction. Prior to each transverse imaging slice of the spin-echo EPI based readouts, navigator and fat suppression were incorporated. Motion data was obtained from the navigator and transmitted back to the sequence, allowing real-time adjustments to slice positioning. The sinc-VSI without velocity-selective gradients during the control condition but with velocity-selective gradients along all three directions during labeling was chosen for the VSASL. The VSASL was compared with pseudo-continuous ASL (pCASL) methods, which selectively tagged the moving spins using a tagging plane placed at the portal vein and hepatic artery.
Results: The motion caused by respiratory activity was effectively computed using the navigator signal. The coefficients of variation (CoV) of average liver voxel in NAV were significantly decreased when compared to breath-hold (BH), with an average reduction of 29.4 ± 18.44% for control images, and 29.89 ± 20.83% for label images ($p < 0.001$). The resulting maps of normalized ASL signal (normalized to M_0) showed significantly higher perfusion weightings in the NAV-compensated VSASL, when compared to the NAV-compensated pCASL techniques.
Conclusions: This study demonstrates the feasibility of using a navigator-based prospective motion compensation technique in conjunction with VSASL for the measurement of liver perfusion without the use of contrast agents while allowing for free-breathing.

Keywords: Velocity selective arterial spin labeling; Liver perfusion; Prospective motion compensation; Navigator-based slice tracking

☆ This work was supported by the Deutsche Forschungsgemeinschaft (DFG, German Research Foundation), 507778062. This study was supported by grants from the German Federal Ministry of Education and Research (BMBF) (82DZL004A1)

* Corresponding author: Felix T. Kurz, Division of Radiology, German Cancer Research Center, 69120 Heidelberg, Germany, and Division of Neuroradiology, Geneva University Hospitals, Geneva, Switzerland.
E-mail addresses: f.kurz@dkfz-heidelberg.de, felixtobias.kurz@hug.ch (F. T. Kurz).

Z Med Phys **35** (2025) 87–97
https://doi.org/10.1016/j.zemedi.2024.06.001
www.elsevier.com/locate/zemedi

Introduction

The human liver receives blood from two sources, namely the portal vein and the hepatic artery, which together constitute its dual blood supply. The portal vein supplies approximately 75% of the blood to the healthy liver, while the hepatic artery provides around 25% of the blood [1–2]. Relative contributions from each vessel are altered distinctly in hepatic diseases, including primary and metastatic liver tumors, liver cirrhosis, and hepatic-renal syndrome [3–4].

Perfusion techniques including contrast agent-based dynamic contrast-enhanced (DCE) and non-contrast based ASL are usually used to access the alteration of these ratios.

Arterial spin labeling (ASL) is a noninvasive and contrast-agent free MRI technique that is gaining popularity for studying liver perfusion. It allows for quantitative assessment of microvascular blood flow or perfusion by utilizing magnetically labeled blood water as a natural tracer [5]. It can be used in patients with contraindications to gadolinium-based contrast agents such as severe renal impairment and allergies to contrast agents, and also avoids potential contrast-agent-related issues such as tissue accumulation of gadolinium [6]. Finally, gadolinium-based contrast agents have a serum elimination half-life on the order of hours even in healthy subjects and a maximum dose, because of which quantitative DCE measurements are not repeatable in short time-frames, nor are they applicable to multiple organs in one examination [7].

ASL, which utilizes magnetically labeled blood water as a naturally occurring tracer, has already gained widespread use in cerebral MRI [8]. Recent developments in ASL technologies, such as pseudo-continuous ASL (pCASL) [9], have provided reliable assessments of cerebral blood flow, e.g., when comparing with H_2O^{15} water PET [10]. However, when applying ASL in liver imaging, respiratory and cardiac motion is a major problem that limits reliability and validity of the acquired perfusion parameters [11]. The B_0 and B_1 inhomogeneities are challenging for pCASL. The selection of the labeling plane, which should be aligned perpendicular to the portal vein is difficult due to the complicated structure of the hepatic vasculature. The portal vein forms at the point where the superior mesenteric vein and splenic vein meet. From there, the portal vein travels upward and toward the right, behind the hepatic artery, until it reaches the liver. pCASL has to label in organ feeding arteries, and the imperfect position of a labeling plane may result in decreased labeling efficiency.

Recently, Velocity Selective Arterial Spin Labeling (VSASL) has been developed, which tags blood according to its speed and produces a magnetic bolus right near the microvasculature in the imaging area. [12]. In contrast to spatially selective pulsed and pCASL approaches, VSASL is insensitive to transit delay effects and no labeling plane was used. Moreover, recent technical advancements have enhanced the labeling efficiency and robustness of VSASL and could increase its potential suitability in various applications where transit delays are a significant concern [12].

The application of pCASL for liver perfusion imaging has been investigated in only a few studies [11,13–14]. To mitigate the issue of motion artifacts during the readout process, images were obtained by implementing a synchronized breathing protocol [11,13]. During this procedure, participants were instructed to follow a breathing pattern in which they took breaths in and out over a period of approximately 4–5 s between two consecutive scans. Additionally, they were asked to hold their breath for approximately 3–6 s while the pCASL spin preparation and data recording took place. The research involved the exploration of liver perfusion imaging without breath-holding, utilizing a navigator-gated balanced steady-state free precession (bSSFP) sequence. Nonrigid image registration was then conducted offline to further enhance the results [14]. However, this technique was limited to acquisition of a single coronal slice. Free-breathing 3D liver ASL has been studied by using prospective motion correction with 2D-EPI navigator and 2D retrospective elastic registration [15]. However, this method suffers from residual fat signal and can not avoid motion during the long 3D acquisition.

To address motion problems, a navigator-based slice tracking technique (NAV) has been incorporated into an Echo-Planar Imaging (EPI) based sequences to prospectively compensate the respiratory motion in renal vascular architecture imaging [16–17] and ASL imaging [18]. Before acquiring each transverse imaging slice in the 2D SE-EPI readouts, navigator and fat suppression were incorporated [19]. In order to determine motion information, the navigator signal saturation caused by EPI excitations was eliminated. The obtained motion information was subsequently incorporated back into the sequence, enabling real-time adjustments of the slice position [19].

In this study, sinc-modulated Velocity Selective Inversion (sinc-VSI) was first applied in healthy volunteers in comparison to pCASL to improve the hepatic perfusion signal. We then investigated the feasibility of this navigator-based prospective motion compensation method in free-breathing VSASL in healthy volunteers for quantification of global perfusion of the liver.

Methods

Subjects

A total of six healthy volunteers (2 women, 4 men) with a mean age of 33 ± 6 years participated in this prospective

examination. The imaging was conducted using an 18-channel body and 16-channel spine receive RF coil on a 1.5T Aera scanner (Siemens Healthineers AG, Erlangen, Germany). The study obtained approval from the institutional ethics committee, and all participants provided written informed consent.

Liver velocity selective ASL and pseudo-continuous ASL imaging

As a navigator, a single gradient-echo slice selection and projection readout were acquired along the inferior-superior (IS) direction through the edge of the diaphragm on the right side. Prior to acquiring each transverse imaging slice in both the 2D SE-EPI based VSASL and pCASL sequences, navigator and fat suppression techniques were applied (Fig. 1). With 50 measurements each, including 32 training navigators (8 measurements) at the beginning of each measurement a whole measurement can be obtained in 5 minutes. Sequence parameters were as follows: TE = 14 ms, FoV = 400 × 240 mm^2, in-plane iPAT factor = 3, partial Fourier = 6/8, matrix size = 120 × 72 × 8, resolution = 3.3 × 3.3 × 8 mm^3, slice gap = 4 mm. For VSASL: labeling/control duration = 64 ms, cutoff velocity V_{cut}=2.8 cm/s. For sinc-VSI, the amplitude of the n_{th} pulse was given by sinc (n/5), where n = −4:1:4. The flip angles of these 9 rectangular pulses add up to 180°. The sinc-VSI was played without VS gradients during control conditions, but with VS gradients along all three directions during labeling as described

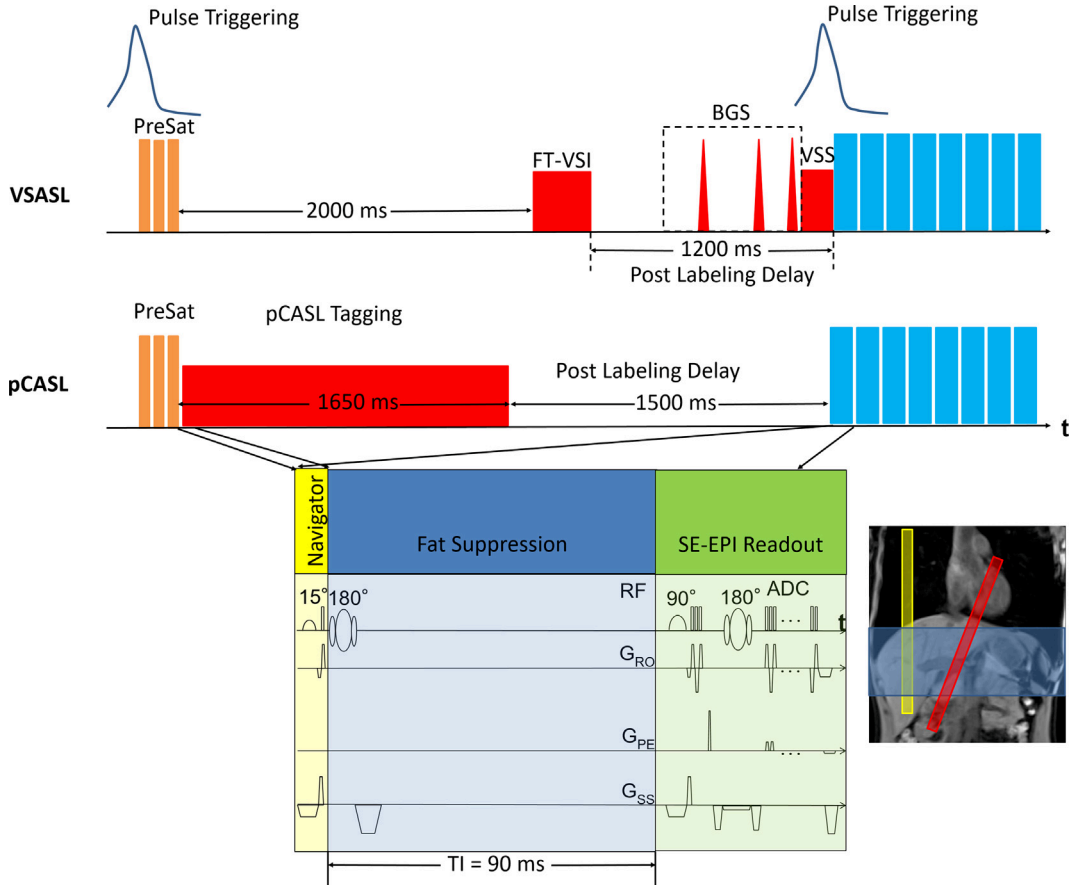

Figure 1. Diagram of the liver VSASL and pCASL sequence. In VSASL, the spins were tagged with Fourier transform based velocity-selective inversion (FT-VSI) label/control pulse trains, combined with slab-selective saturation pulses (PreSat), nonselective background suppression (BGS) pulses during the post labeling delay, and a VS saturation (VSS) for suppressing large-vessel signal followed by the readout. To track motion, a navigator was utilized via a solitary gradient-echo slice selection and projection readout, situated at the position of the diaphragm in the inferior-superior direction. Before acquiring each transverse imaging slice in the spin-echo 2D EPI sequence, the navigator was acquired, and fat suppression was applied. During the systolic period, the pulse signal triggered the labeling pulse train and readout. In order to target the hepatic blood flow, a tagging plane was positioned at both the portal vein and hepatic artery in the case of pCASL (colored in red). The navigator was positioned at a perpendicular angle to the diaphragm (highlighted in yellow), while the imaging volume was adjusted to encompass the kidneys (depicted in blue).

in a previous study [20]. The advantage of this setting is that they show good resistance to B_0 and B_1 inhomogeneity. Delay between the pre-saturation and the labeling modules = 2 s, post-labeling delay (PLD) =1200 ms, TR_{NAV}/ TR_{BH} = 5/7 s, timing for background suppression (BGS) = 444 ms, 719 ms and 1118 ms; For pCASL: labeling duration = 1650 ms, PLD = 1500 ms, TR = 5 s, TI for SPAIR (SPectral Attenuated Inversion Recovery) fat suppression = 90 ms, FoV_{nav} = 200 × 200 × 10 mm^3, res_{nav} = 64, flip $angle_{nav}$ = 15°, TR_{nav} = 4.22 ms (Fig. 1). The blood pulse signal served as the trigger for the labeling pulse train and readout, occurring exclusively during the systolic period as recommended [21]. The pulse signal was acquired at the fingertip. In order to label the global liver blood flow, the tagging plane was positioned almost perpendicular to the portal vein (PV) and hepatic artery (HA), as illustrated in Fig. 1.

To evaluate the characteristics of pulse trains using Fourier transform based velocity-selective inversion (FT-VSI), numerical simulations were conducted using matrix rotation based on the Bloch equations using MATLAB (MathWorks, Inc., Natick, MA, USA). The M_z profile in the presence of B_1 of 1 and B_0 of 0, with arterial T_1 (1500 ms) and T_2 (200 ms) relaxation were simulated.

In the following sections, we referred to the reference method as "breath-hold" (BH), which involved performing VSASL scans with a timed breathing protocol. During the BH procedure, we conducted VSASL labeling and incorporated PLD and 2D SE-EPI readout. The participants were instructed to inhale deeply and subsequently maintain breath-holding until the attainment of a repetition time (TR) of 7000 ms. With such a TR, each repetition provided 2870 ms for deep inspiration and expiration.

Motion analysis

We utilized the initial 32 acquired navigator signals as navigators for training purposes. Since eight slices were acquired in each TR, this corresponds to the navigators from the first four repetitions. Due to the signal saturation caused by the transverse imaging excitation of SE-EPI there would be signal voids (negative peaks) in the navigator signal. First, we truncated the signal after identifying the peaks from the averaged training navigators. To enhance the signal-to-noise ratio (SNR), we combined the signals from multiple coils located near the diaphragm. Coil clustering [22] was implemented on the training navigator data to identify the appropriate coil elements. For a comprehensive description of the motion analysis, please refer to previous studies [19]. Only motion in the up-down direction was derived from the navigator signal.

Real-time adjustments were made to the sequence and slice positioning by sending the motion information directly back to the system. The motion analysis and real-time feedback were carried out on the scanner using ICE (Image Calculation Environment, Siemens Healthineers AG, Erlangen, Germany).

Data processing

For VSASL evaluations, the hepatic blood flow (HBF) was calculated by [12]:

$$HBF = \frac{6000 \cdot \lambda \cdot \Delta M \cdot exp(TI/T_{1b})}{2\alpha \cdot \tau \cdot M_0 \cdot SI_B},$$
$$SI_B = 1 - exp(-T_{sat}/T_{1b}),$$

with ΔM being the difference between the control and label, M_0 representing equilibrium magnetization, which was measured separately without saturation and labeling scheme, α as the tagging efficiency ($\alpha = 0.95$) [23], TI as the time between labeling pulse and readout, which was 1.2 s, T_{1b} =1.2 s as the longitudinal blood relaxation rate [24], λ as the blood/tissue water partition coefficient ($\lambda = 0.9$ ml/g), τ as the bolus duration (1.176 s), and saturation duration T_{sat} as 2 s.

For pCASL evaluations, the hepatic blood flow (HBF) was calculated as:

$$HBF = \frac{6000 \cdot \lambda \cdot \Delta M \cdot exp(PLD/T_{1b})}{2\alpha \cdot T_{1b} \cdot M_0 \cdot [1 - exp(-\tau/T_{1b})]},$$

with α as the tagging efficiency ($\alpha = 0.86$), PLD = 1.5 s, and labeling RF duration time τ as 1.65 s.

For comparison of normalized ASL signal and HBF, the M_0 map was segmented (masked) by thresholding and registered to the first time point of each ASL measurement.

Evaluation of PMC impact

In order to assess the effects of prospective motion correction on image quality, we calculated the coefficients of variation (CoV) as follows: for each voxel in every slice of the liver region of interest (ROI), we derived a series of time-dependent signal intensity values, and determined the corresponding mean and standard deviation values for each time series. The CoV was calculated by dividing the standard deviation of the time series by the mean value of the corresponding voxel [25]. Subsequently, for each volunteer, we computed the average CoV value across all voxels within the liver ROIs for both the control and label images.

Statistical analyses

For assessing the normality of voxel intensity distributions, we utilized the one-sample Kolmogorov-Smirnov test

in MATLAB. When comparing distributions in pairs, paired t-tests were conducted if both distributions followed a standard normal distribution; otherwise, a signed Wilcoxon rank test was employed. The significance level for all tests was set at $p < 0.05$. The reported results indicate the mean value, with the standard deviation denoted by the symbol ±.

Results

We simulated velocity response of rect-VSI and sinc-VSI under the label (solid red curves) and the control (dashed red curves) conditions in Fig. 2. Both rect-VSI and sinc-VSI pulses demonstrated the ability to label spins within a narrow velocity range. However, the sinc-VSI pulse exhibited a smoother response in the "unperturbed" velocity bands. The supplementary figure Fig. S1 visualizes that navigator signals can be utilized to calculate respiratory motion. Motion information of diaphragm were precisely overlaid on the navigator signals. Furthermore, we generated spatial CoV maps for liver voxels in control images of a representative volunteer, as shown in Fig. 3a. The CoV maps in NAV and BH were comparable, although the top slices of BH displayed typical ring artifacts caused by respiratory motion. Moreover, there was a slight reduction in CoV values in NAV when compared to BH (Fig. 3b, c). The average CoV values in NAV were considerably lower than those in BH, with an average reduction of 29.4 ± 18.44% for control images and 29.89 ± 20.83% for label images ($p < 0.001$).

The resulting maps of normalized ASL signal (normalized to M_0) showed higher perfusion weightings in the NAV-compensated VSASL, when compared to the BH VSASL and NAV-compensated pCASL techniques, see Fig. 4 and Table 1. In the case of BH and NAV acquisitions, a more intricate vascular structure can be observed in the VSASL signal maps. This can be seen, for instance, in Fig. 4, specifically in the upper two rows depicting a representative subject (Subject 5).

We calculated HBF maps and determined mean HBF values for six healthy volunteers in the liver, see Fig. 5 and Table 2. In general, BF values are higher in kidney than in liver as presented in Fig. 5. HBF values are less noisy in NAV-compensated VSASL. More homogenous HBF can be found in NAV-compensated VSASL.

The mean normalized ASL signals across all subjects and all measurements were 1.78 ± 0.79% in the BH VSASL and 1.47 ± 0.43% in the NAV-compensated VSASL, which were higher than in the NAV-compensated pCASL (Table 1). There were significant differences between NAV VSASL and NAV pCASL (1.47 ± 0.43 vs 0.71 ± 0.52) (Fig. 6a**)**.

Table 2 shows the mean HBF value across all subjects and all measurements with 78.10 ± 22.78 ml/100 g/min in the NAV-compensated VSASL, which was lower than the BH VSASL (95.04 ± 42.23 ml/100 g/min), and larger than NAV-compensated pCASL values (86.24 ± 64.01 ml/100 g/min). These differences were, however, not significant (Fig. 6b**)**.

To compare the intensity distribution of normalized ASL signal and HBF, the histograms are plotted in Fig. 7, showing the different ASL methods (BH VSASL, NAV VSASL and NAV pCASL).

Discussion

In this work, a sinc-VSI was played out without VS gradients during control condition, but with VS gradients along all three directions during labeling for a higher SNR efficiency. The developed navigator-based ASL SE-EPI readout slice tracking technique successfully compensates respiratory motion in real-time. We specifically found that (i), the mean CoV values in NAV showed a significant reduction compared to BH, (ii), the normalized ASL signal showed significantly higher perfusion weightings in the NAV-compensated VSASL, when compared to NAV-compensated pCASL techniques, and (iii), that HBF values, on the other hand, were not significantly different across different methods.

When compared to the case with BH, we could see that the NAV method provides significantly lower CoV values. Due to the different depths of each BH during the measurements, the BH method is only of limited use as a reference for comparison with the NAV method.

Normalized ASL signals showed that BH VSASL and NAV VSASL provide significantly higher perfusion weightings than the NAV pCASL approach (Fig. 4**,** Fig. 6a and Table 1). However, the differences between measurements using the same method were not significant. HBF values, on the other hand, were not significantly different across different methods; however, the standard deviations of NAV VSASL were lower, indicating a more stable acquisition method for providing HBF values.

Compared to BH VSAL, the NAV VSASL showed a broader distribution in both normalized signal and HBF (Fig. 7). This variation might be due to the residue motion in our navigator technique. The distribution of normalized signals from NAV pCASL also showed a shift to lower values compared to BH VSASL, indicating VSASL produces higher perfusion weightings. According to the histogram of HBF and Fig.5, BH VSASL delivered the most homogenous perfusion in the liver and thus the most robust evaluation of HBF.

This study is the first study that utilizes VSASL for the whole liver ASL perfusion assessment. The advantage of this technique has been observed in a stroke study, since it is less sensitive to the selection of the labeling delay [26]. Another advantage of VSASL in liver ASL is that it is not

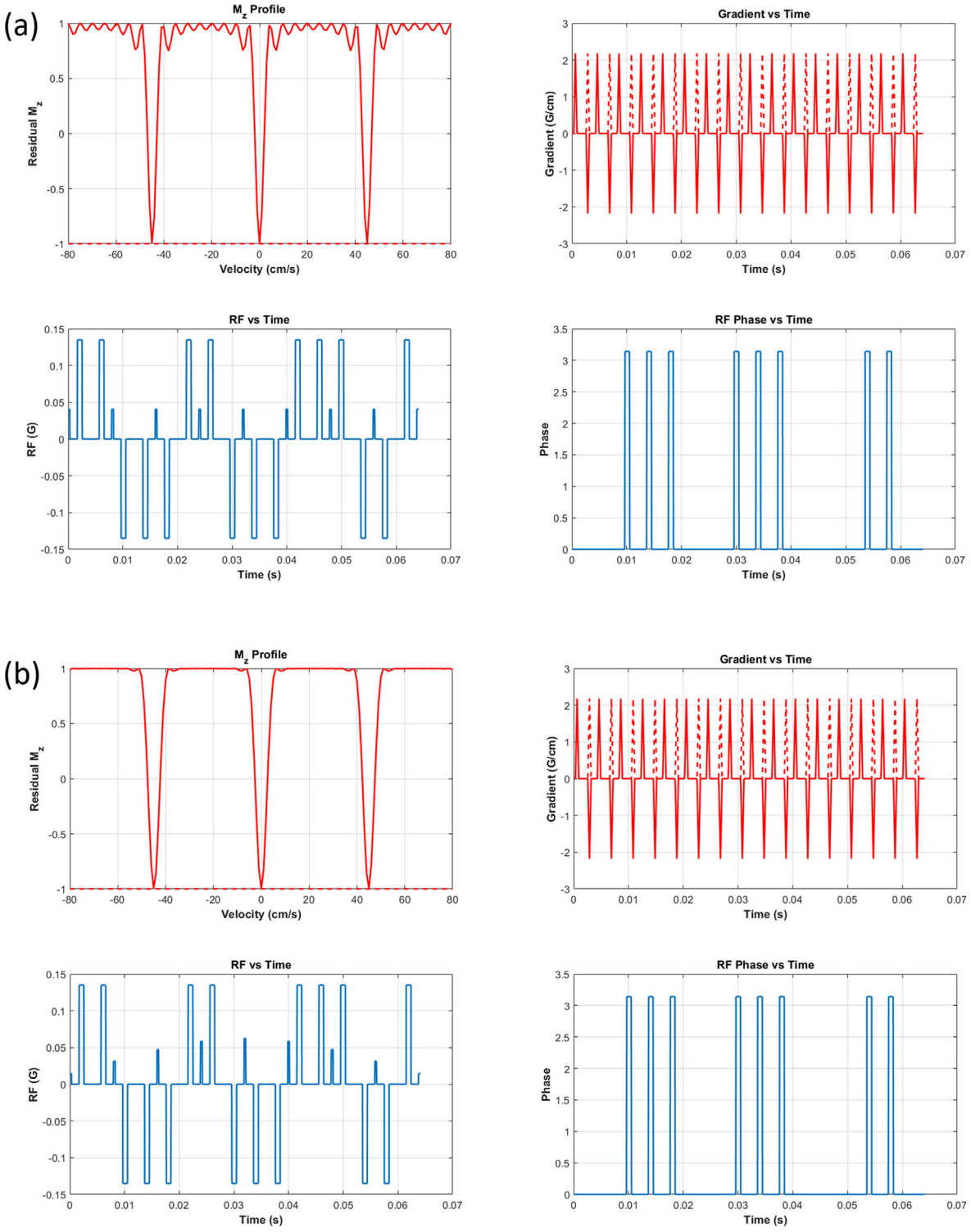

Figure 2. Simulated velocity response of rect-VSI (a) and sinc-VSI (b) under the label (solid red curves) and the control (dashed red curves) conditions. The RF pulse, phase of RF pulse and gradient for the FT-VSI labeling (solid) and control (dashed) are plotted. No B_1 or B_0 inhomogeneity were considered for these simulations.

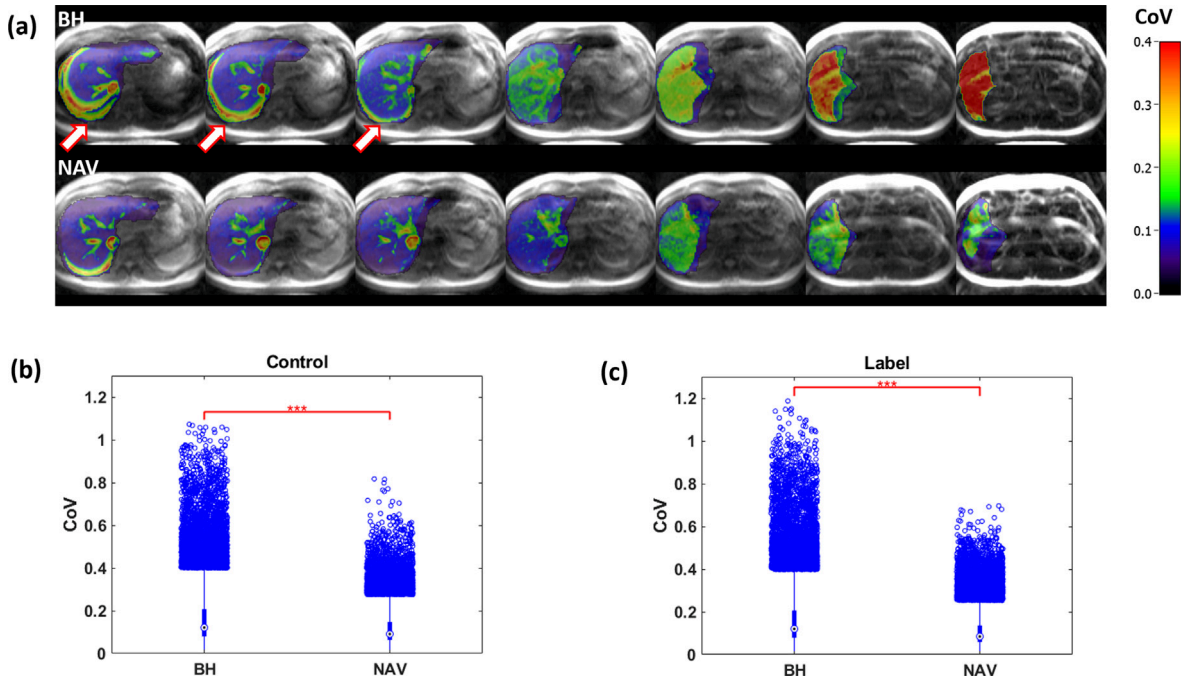

Figure 3. (a) Maps of the coefficient of variation (CoV) of the liver in subject 2. The CoV values were calculated based on the temporal variations in signal intensity of each voxel within the liver during breath-hold (BH) and navigator-based slice tracking (NAV). The mean CoV values during NAV were significantly lower than those during BH, with an average a reduction of 29.4 ± 18.44% for control images, and 29.89 ± 20.83% for label images ($p<0.001$). Typical ring artifacts (red arrow) due to residual respiratory motion can be found in BH.

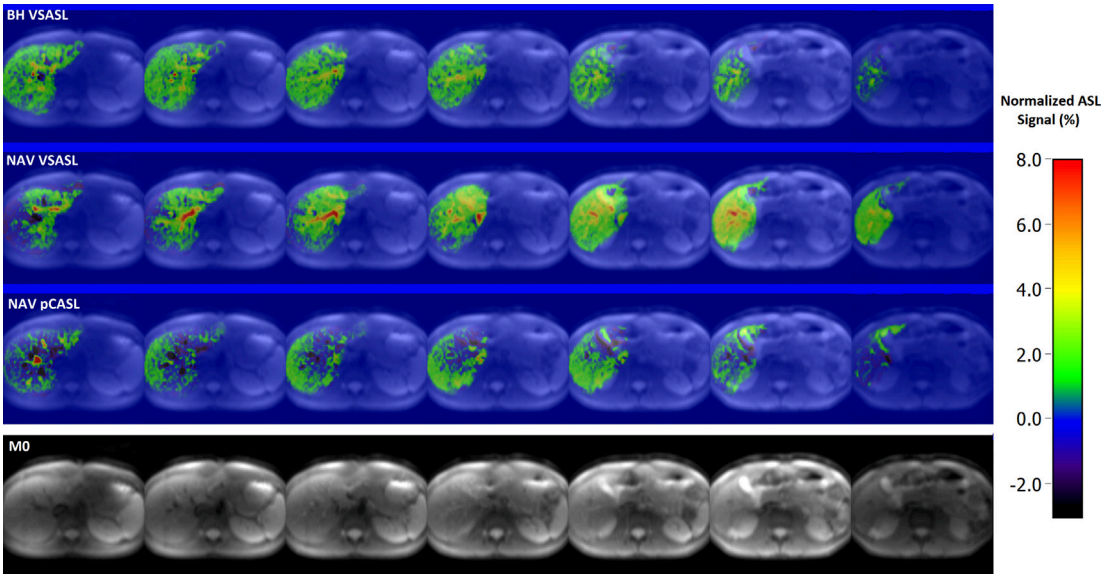

Figure 4. Comparison of the relative signal change due to the label (normalized to the spin density image) between breath-hold (BH VSASL), navigator-based slice tracking (NAV VSASL), NAV pCASL from one representative subject (subject5). In the case of BH and NAV VSASL, more intricate details can be observed in the ASL signal maps. The VSASL signal maps showed a more intricate vascular structure in both BH and NAV cases. Due to the different slice position of M_0 (measured during BH) and the perfusion weighted images, the BH VSASL is truncated after normalization (right-hand-side in second row).

Table 1
Normalized ASL signal (%) for healthy volunteers (N = 6) during breath-hold (BH VSASL), navigator-based slice tracking (NAV VSASL), NAV pCASL.

	BH VSASL	NAV VSASL	NAV pCASL
1	0.96 ± 0.02	1.20 ± 0.03	0.56 ± 0.02
2	3.00 ± 0.03	1.90 ± 0.04	0.53 ± 0.05
3	2.31 ± 0.03	1.08 ± 0.02	0.26 ± 0.02
4	2.00 ± 0.03	1.01 ± 0.02	0.64 ± 0.03
5	1.23 ± 0.02	1.61 ± 0.03	0.50 ± 0.03
6	1.20 ± 0.02	1.99 ± 0.03	1.74 ± 0.04
Mean	1.78 ± 0.79	1.47 ± 0.43	0.71 ± 0.52

Table 2
Hepatic blood flow (mL/100 g/min; mean ± std) for healthy volunteers (N = 6) during breath-hold (BH VSASL), navigator-based slice tracking (NAV VSASL), NAV pCASL.

	BH VSASL	NAV VSASL	NAV pCASL
1	51.31 ± 1.07	63.72 ± 1.51	68.19 ± 2.28
2	160.07 ± 1.67	101.06 ± 2.13	65.24 ± 6.16
3	123.16 ± 1.62	57.66 ± 1.20	31.85 ± 2.56
4	106.47 ± 1.48	53.89 ± 1.03	77.93 ± 3.28
5	65.47 ± 1.10	85.96 ± 1.74	61.23 ± 3.70
6	63.74 ± 1.21	106.30 ± 1.40	213.00 ± 5.25
Mean	95.04 ± 42.23	78.10 ± 22.78	86.24 ± 64.01

sensitive to the selection of the labeling plane and movement of the labeling plane.

While V_{cut} recommended in literature was 2 cm/s [12], we used 2.8 cm/s. Lower V_{cut} will also result in higher flow-sensitivity: Only arterial blood decelerated below V_{cut} after labeling generates measurable ASL signal [12]. Therefore, higher V_{cut} produces a stronger perfusion signal.

The advantage of axial slice acquisitions is that they allow smaller FOVs, and thus higher image resolution, therefore reducing the risk of changes in magnetization used by a navigator, such as for retrospective image sorting.

To date, only a limited number of ASL studies have been conducted on human liver perfusion, utilizing various ASL techniques (continuous and pulsed), tagging planes, and mathematical models for processing measured signal data. Consequently, there are variations in the reported perfusion values [13]. As reported in previous studies, global (90 ± 1 ml/100 g/min), arterial (21 ± 5 ml/100 g/min), and portal-venous (69 ± 5 ml/100 g/min) HBF perfusion values were acquired in the healthy human liver using a pCASL technique, and our results of three perfusions and ratios agree with previous studies [11,13,27]. DCE measurements can be used in future studies to verify our results.

One limitation of this study is that motion compensation was only performed in the inferior-superior direction of the diaphragm using a one-dimensional navigator. Correction for motion in the anterior-posterior direction could be implemented by incorporating an additional navigator, but this would result in increased measurement and reconstruction time. In-plane motion could also be corrected retrospectively [28], or a two-dimensional navigator could be utilized for fast and precise motion correction [29]. Inhomogeneity

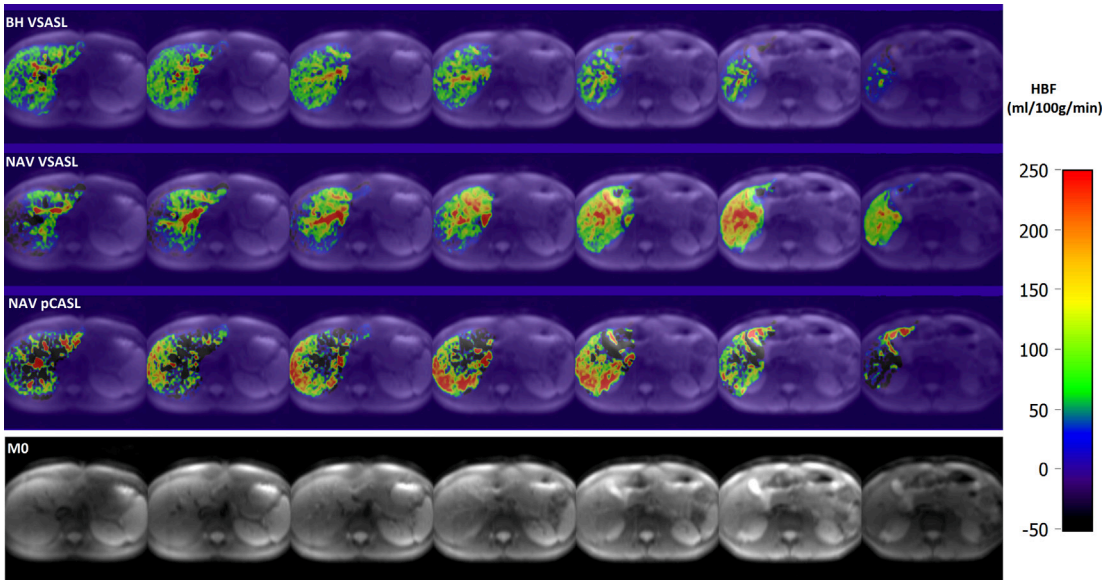

Figure 5. Comparison of quantitative hepatic blood flow (HBF) maps between breath-hold (BH VSASL), navigator-based slice tracking (NAV VSASL), NAV pCASL from the same representative subject (subject5). In general, HBF values are higher in kidney than in liver, as shown. HBF is less noisy in NAV-compensated VSASL. More homogenous HBF can be found in NAV-compensated VSASL.

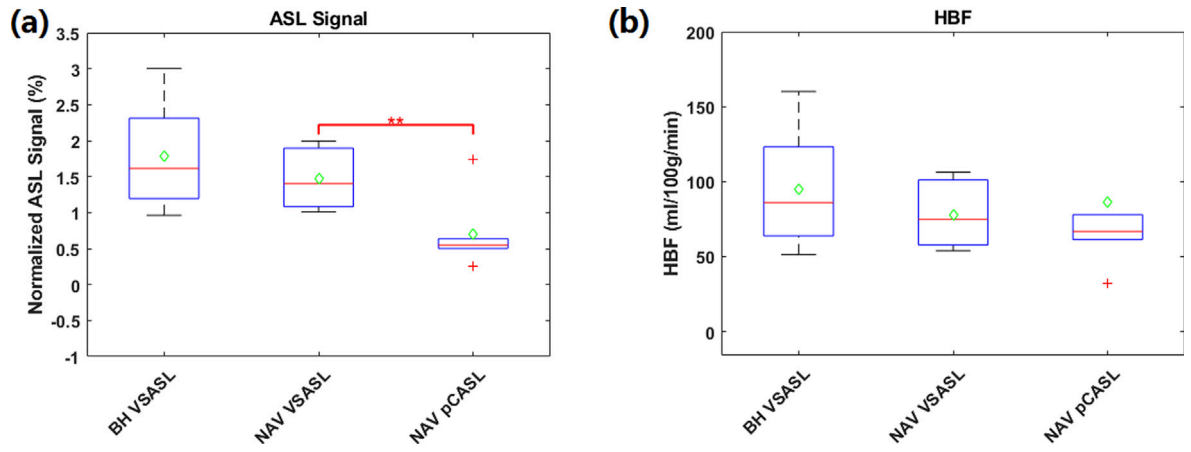

Figure 6. (a) Comparison of averaged ASL signal per voxel across subjects (normalized to the spin density image; n=6) between breath-hold (BH VSASL), navigator-based slice tracking (NAV VSASL), NAV pCASL, and (b) comparison of averaged HBF values per voxel across subjects, see also Tables 1, 2. Red line: median value, green dot: mean value.

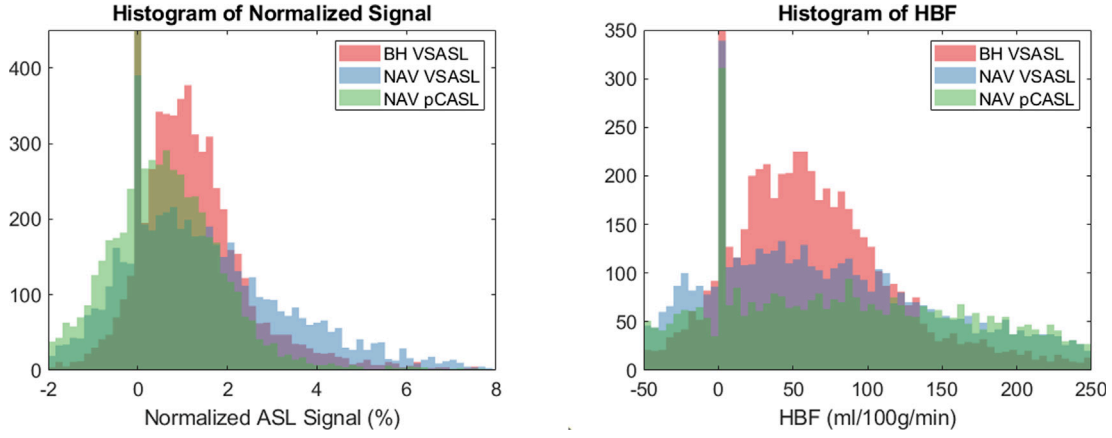

Figure 7. Histograms of normalized signal and HBF from different methods including BH VSASL (pink), NAV VSASL (blue) and NAV pCASL (green).

could affect the perfusion assessment. M_0, control and label images may contain B1 inhomogeneities. But since the inhomogeneous subtracted signal ΔM was normalized using (divided by) similarly inhomogeneous M_0, this B1 effect in normalized signal should be reduced (**Supplementary** Fig. S2). Fig.S2b shows the measured signal along an anterior-posterior projection to demonstrate this: The normalized signal along this line has smaller fluctuation than that of ΔM, indicating that the inhomogeneity is reduced after normalization. Correct for magnetic transfer (MT) effects and profile issues of excitation and refocusing pulse could be considered in the readout. The labeling efficiencies used for the calculation of HBF were defined according to the values in literature of brain studies [23]. Since no other adequate values were available in future, these parameters should be verified by further measurements.

To differentiate between portal-venous and arterial perfusion, it is possible to perform separate measurements for labeling blood flow into the liver and selective labeling of arterial blood flow. The venous part can be extracted by subtracting these two measurements. The global liver blood flow can be labeled using VSASL due to its high SNR efficiency. Furthermore, to selectively tag arterial blood flow in the hepatic artery, a tagging plane can be positioned cranial to the diaphragm. This placement allows for the labeling of arterial blood in the descending aorta using pCASL. Since the aim of this study is to find the best performance of global liver perfusion, arterial perfusion was not performed. The disadvantage of VSASL is that separation of arterial and venous perfusion of the liver is not possible.

Using an ECG signal could lead to higher accuracy of cardiac triggering. However, for the proof of concept study,

the pulse signal was easier to acquire. One simulation [21] suggests that the optimal moment of triggering lies at the end-systolic phase, which corresponds to a delay of 0 ms with the finger pulse-oxy trigger.

For ASL, the short T_1 relaxation time in the blood (1.2 s at 1.5T,) limits the readout time. Thus, a faster readout such as multiband (MB)-EPI [30–32], which promises multiple-slices and higher perfusion sensitivity, would be preferable .

Conclusion

To summarize, this study demonstrates the feasibility of liver VSASL combined with a prospective motion compensation technique for free-breathing liver perfusion measurement without contrast agent.

CRediT authorship contribution statement

Ke Zhang: Conceptualization, Data curation, Formal analysis, Funding acquisition, Investigation, Methodology, Resources, Software, Validation, Visualization, Writing – original draft, Writing – review & editing. **Simon M.F. Triphan:** Methodology, Resources, Software, Writing – review & editing. **Mark O. Wielpütz:** Funding acquisition, Writing – review & editing. **Christian H. Ziener:** Data curation, Writing – review & editing. **Mark E. Ladd:** Project administration, Writing – review & editing, Resources. **Heinz-Peter Schlemmer:** Project administration, Writing – review & editing, Resources. **Hans-Ulrich Kauczor:** Project administration, Writing – review & editing, Resources. **Oliver Sedlaczek:** Data curation, Writing – review & editing, Project administration, Resources. **Felix T. Kurz:** Data curation, Funding acquisition, Project administration, Resources, Supervision, Writing – review & editing.

Data Availability Statement

The code used to extract the data is distributed by the authors as open-source. The patient data can be made available on request due to privacy/ethical restrictions.

Declaration of competing interest

The authors declare that they have no known competing financial interests or personal relationships that could have appeared to influence the work reported in this paper.

Appendix A Supplementary data

Supplementary data to this article can be found online at https://doi.org/10.1016/j.zemedi.2024.06.001.

References

[1] Schenk WG, Drapanas T, Mcdonald K, Mcdonald JC. Direct measurement of hepatic blood flow in surgical patients - with related observations on hepatic flow dynamics in experimental animals. Ann Surg 1962;156(3):463–1000.
[2] Chiandussi L, Greco F, Sardi G, Vaccarino A, Ferraris CM, Curti B. Estimation of hepatic arterial and portal venous blood flow by direct catheterization of vena porta through umbilical cord in man. Preliminary Results. Acta Hepato-Splenol 1968;15(3):166-+.
[3] Pandharipande PV, Krinsky GA, Rusinek H, Lee VS. Perfusion imaging of the liver: current challenges and future goals. Radiology 2005;234(3):661–673.
[4] Kim SH, Kamaya A, Willmann JK. CT perfusion of the liver: principles and applications in oncology. Radiology 2014;272(2):321–343.
[5] Taso M, Aramendia-Vidaurreta V, Englund EK, Francis S, Franklin S, Madhuranthakam AJ, et al., Group IPS. Update on state-of-the-art for arterial spin labeling (ASL) human perfusion imaging outside of the brain. Magn Reson Med 2023;89(5):1754–76.
[6] Davies J, Siebenhandl-Wolff P, Tranquart F, Jones P, Evans P. Gadolinium: pharmacokinetics and toxicity in humans and laboratory animals following contrast agent administration. Arch Toxicol 2022;96(2):403–429.
[7] Aronhime S, Calcagno C, Jajamovich GH, Dyvorne HA, Robson P, Dieterich D, et al. DCE-MRI of the liver: effect of linear and nonlinear conversions on hepatic perfusion quantification and reproducibility. J Magn Reson Imaging 2014;40(1):90–98.
[8] Wang X, Bishop C, O'Callaghan J, Gayhoor A, Albani J, Theriault W, et al. MRI assessment of cerebral perfusion in clinical trials. Drug Discov Today 2023;28(4):103506.
[9] Dai WY, Garcia D, de Bazelaire C, Alsop DC. Continuous flow-driven inversion for arterial spin labeling using pulsed radio frequency and gradient fields. Magn Reson Med 2008;60(6):1488–1497.
[10] Zhang K, Herzog H, Mauler J, Filss C, Okell TW, Kops ER, et al. Comparison of cerebral blood flow acquired by simultaneous [15O] water positron emission tomography and arterial spin labeling magnetic resonance imaging. J Cereb Blood Flow Metab 2014;34(8):1373–1380.
[11] Martirosian P, Pohmann R, Schraml C, Schwartz M, Kuestner T, Schwenzer NF, et al. Spatial-temporal perfusion patterns of the human liver assessed by pseudo-continuous arterial spin labeling MRI. Z Med Phys 2019;29(2):173–183.
[12] Qin Q, Alsop DC, Bolar DS, Hernandez-Garcia L, Meakin J, Liu D, et al., Group ISS. Velocity-selective arterial spin labeling perfusion MRI: A review of the state of the art and recommendations for clinical implementation. Magn Reson Med 2022;88(4):1528–47.
[13] Schalkx HJ, Petersen ET, Peters NHGM, Veldhuis WB, van Leeuwen MS, Pluim JPW, et al. Arterial and portal venous liver perfusion using selective spin labelling MRI. Eur Radiol 2015;25(6):1529–1540.
[14] Pan XL, Qian TY, Fernandez-Seara MA, Smith RX, Li KC, Ying K, et al. Quantification of liver perfusion using multidelay pseudocontinuous arterial spin labeling. J Magn Reson Imaging 2016;43(5):1046–1054.
[15] Huber J, Gunther M, Channaveerappa M, Hoinkiss DC. Towards free breathing 3D ASL imaging of the human liver using prospective motion correction. Magn Reson Med 2022.
[16] Zhang K, Triphan S, Kurz F, Ziener C, Schlemmer H, Kauczor H, et al. Navigator-triggered kidney vessel architecture imaging. ISMRM2021. p. 2537.
[17] Zhang K, Triphan SMF, Kurz FT, Ziener CH, Kauczor HU, Schlemmer HP, et al. Navigator-based slice tracking for prospective

motion correction in kidney vessel architecture imaging. Magn Reson Imaging 2023;98:26–35.
[18] Zhang K, Triphan S, Kurz F, Ziener C, Kauczor H, Schlemmer H, et al. Navigator-based slice tracking for kidney pCASL using EPI acquisition. London: ISMRM; 2022. p. 3949.
[19] Zhang K, Triphan SMF, Ziener CH, Jende JME, Kauczor HU, Schlemmer HP, et al. Navigator-based slice tracking for kidney pCASL using spin-echo EPI acquisition. Magn Reson Med 2023;90 (1):231–239.
[20] Zhang K, Triphan SMF, Ziener CH, Kauczor HU, Schlemmer HP, Sedlaczek O, et al. Comparison of velocity-selective-inversion arterial spin labeling schemes. ISMRM2023. p. 2906.
[21] Verbree J, van Osch MJP. Influence of the cardiac cycle on pCASL: cardiac triggering of the end-of-labeling. MAGMA 2018;31 (1):223–233.
[22] Zhang T, Cheng JY, Chen YX, Nishimura DG, Pauly JM, Vasanawala SS. Robust self-navigated body MRI using dense coil arrays. Magn Resonance Med 2016;76(1):197–205.
[23] Liu D, Xu F, Li W, van Zijl PC, Lin DD, Qin Q. Improved velocity-selective-inversion arterial spin labeling for cerebral blood flow mapping with 3D acquisition. Magn Reson Med 2020;84(5): 2512–2522.
[24] Wang JJ, Alsop DC, Song HK, Maldjian JA, Tang K, Salvucci AE, et al. Arterial transit time imaging with flow encoding arterial spin tagging (FEAST). Magn Reson Med 2003;50(3):599–607.
[25] Callaghan MF, Josephs O, Herbst M, Zaitsev M, Todd N, Weiskopf N. An evaluation of prospective motion correction (PMC) for high resolution quantitative MRI. Front Neurosci 2015;9:97.
[26] Qiu D, Straka M, Zun Z, Bammer R, Moseley ME, Zaharchuk G. CBF measurements using multidelay pseudocontinuous and velocity-selective arterial spin labeling in patients with long arterial transit delays: comparison with xenon CT CBF. J Magn Reson Imaging 2012;36(1):110–119.
[27] He X, Gumus S, Bae KT. Assessing Portal Vein Contribution on Hepatic Perfusion based on Arterial Spin Labeling MRI. ISMRM2014. p. 0377.
[28] Slipsager JM, Glimberg SL, Hojgaard L, Paulsen RR, Wighton P, Tisdall MD, et al. Comparison of prospective and retrospective motion correction in 3D-encoded neuroanatomical MRI. Magn Reson Med 2021.
[29] Skare S, Hartwig A, Martensson M, Avventi E, Engstrom M. Properties of a 2D fat navigator for prospective image domain correction of nodding motion in brain MRI. Magn Reson Med 2015;73(3):1110–1119.
[30] Zhang K, Yun SD, Triphan SMF, Sturm VJ, Buschle LR, Hahn A, et al. Vessel architecture imaging using multiband gradient-echo/spin-echo EPI. Plos One 2019;14(8):e0220939.
[31] Zhang K, Yun SD, Shah NJ. Tripled readout slices in multi time-point pCASL using multiband look-locker EPI. Plos One 2015;10 (11):e0141108.
[32] Zhang K, Sturm VJ, Buschle LR, Hahn A, Yun SD, Jon Shah N, et al. Dual-contrast pCASL using simultaneous gradient-echo/spin-echo multiband EPI. Magn Reson Imaging 2019;57:359–367.